



HAL
open science

First record of early Aptian Oceanic Anoxic Event 1a from the Paris Basin (France) - Climate signals on a terrigenous shelf

Jean-François Deconinck, Danny Boué, Francis Amédéo, François Baudin, Ludovic Bruneau, Emilia Huret, Philippe Landrein, Jean-David Moreau, Anne-Lise Santoni

► To cite this version:

Jean-François Deconinck, Danny Boué, Francis Amédéo, François Baudin, Ludovic Bruneau, et al.. First record of early Aptian Oceanic Anoxic Event 1a from the Paris Basin (France) - Climate signals on a terrigenous shelf. *Cretaceous Research*, 2021, 125, pp.104846. 10.1016/j.cretres.2021.104846 . hal-03222734

HAL Id: hal-03222734

<https://hal.science/hal-03222734v1>

Submitted on 9 May 2023

HAL is a multi-disciplinary open access archive for the deposit and dissemination of scientific research documents, whether they are published or not. The documents may come from teaching and research institutions in France or abroad, or from public or private research centers.

L'archive ouverte pluridisciplinaire **HAL**, est destinée au dépôt et à la diffusion de documents scientifiques de niveau recherche, publiés ou non, émanant des établissements d'enseignement et de recherche français ou étrangers, des laboratoires publics ou privés.



Distributed under a Creative Commons Attribution - NonCommercial 4.0 International License

1 **First record of early Aptian Oceanic Anoxic Event 1a from the Paris Basin (France) -**
2 **climate signals on a terrigenous shelf**

3

4 Jean-François Deconinck¹, Danny Boué¹, Francis Amédéo^{1,2}, François Baudin³, Ludovic
5 Bruneau¹, Emilia Huret⁴, Philippe Landrein⁴, Jean-David Moreau¹ and Anne Lise Santoni¹

6

7 ¹ Biogéosciences, UMR 6282, uB/CNRS, Université de Bourgogne/Franche-Comté, 6
8 Boulevard Gabriel, 21000 Dijon, France.

9 ² 26 rue de Nottingham, 62100 Calais, France.

10 ³ IStEP, UMR 7193, SU/CNRS, Sorbonne Université, 4 Place Jussieu, 75005 Paris, France.

11 ⁴ Agence Nationale pour la gestion des déchets radioactifs, Centre de Meuse/Haute-Marne,
12 RD 960, 55290 Bure, France.

13

14 Abstract

15 In 2013, Andra (French National Radioactive Waste Management Agency) drilled boreholes
16 to the south-east of the Paris Basin, to characterise Aptian and Albian clayey formations,
17 including the ‘Argiles à Plicatules’ Formation dated as early Aptian. One of these boreholes
18 intersected this formation with an excellent recovery allowing detailed biostratigraphy
19 (ammonites), sedimentology, clay mineralogy, isotope geochemistry ($\delta^{13}\text{C}_{\text{org}}$) and Rock-Eval
20 analyses to be performed. The base of the formation corresponds to transgressive dark-grey
21 silty clays with iron oolites and plant debris indicating a coastal environment evolving up-
22 section to upper offshore environments. Higher in the succession, clays with less than 4%
23 CaCO_3 and less than 0.8% of organic matter were deposited in lower offshore environments.
24 The occurrence of ammonites can be used to draw a biostratigraphic scheme, and in
25 particular, to recognise the *deshayesi* and *furcata* ammonite Zones.

26 The clay mineral assemblages are composed of illite and kaolinite associated with minor
27 amounts of chlorite, vermiculite and smectite. The $\delta^{13}\text{C}_{\text{org}}$ values range between -24 and -
28 25‰ except in a particular interval characterised by a prominent negative excursion of about -
29 3‰, that is recognised worldwide and precedes Oceanic Anoxic Event 1a (OAE1a). This
30 interval is also characterised by an abundance of kaolinite and the absence of smectite
31 suggesting an acceleration of the hydrological cycle and enhanced runoff and hydrolysing
32 conditions over the emerged landmasses just before and during the onset of OAE1a. This
33 climate change is consistent with isotope and palynological data indicating warm and humid
34 climate conditions before and during the onset of OAE1a. Surprisingly, the interval
35 corresponding to OAE1a is not significantly enriched in organic matter and its lithology is not
36 different from the rest of the core suggesting that Tethyan anoxic water masses did not reach
37 the relatively shallow epicontinental environments of the Paris Basin.

38

39 Keywords: Lower Cretaceous, Aptian, Oceanic Anoxic Event, Paris Basin, Clay minerals,
40 Organic carbon isotopes

41

42

43 Introduction

44 Identified for the first time by Schlanger and Jenkyns (1976), Oceanic Anoxic Event
45 (OAE) 1a (early Aptian) is characterised by the worldwide preservation of organic matter in
46 black shales as a consequence of intensification in marine primary productivity under oceanic
47 oxygen-depleted conditions (Coccioni et al., 1987; 1992; Erba, 1994, Erba, 2004; Erbacher et
48 al., 1996; Leckie et al., 2002; Jenkyns, 2010; Föllmi, 2012; Erba et al., 2015). A global
49 perturbation in the carbon cycle is associated with this event, recorded by a prominent
50 negative excursion followed by a shift towards more positive values (Menegatti et al., 1998).

51 The negative excursion is generally explained by an intense volcanic episode at the origin of
52 the formation of the Ontong-Java oceanic plateau (Tarduno et al., 1991; Larson and Erba,
53 1999; Méhay et al., 2009; Tejada et al., 2009; Bottini et al., 2012; Erba et al., 2015;
54 Charbonnier and Föllmi, 2017) while the following positive excursion is seen as a
55 consequence of organic matter burial in oceanic sediments. The duration of the negative
56 excursion, first underestimated between 27 and 44 kyr (Li et al., 2008), is likely longer with a
57 duration estimated between 280 and 350 kyr (Lorenzen et al., 2013). The duration of OAE1a
58 itself is estimated between 1 and 1.3 myr (Li et al., 2008). These environmental changes were
59 associated with rising sea surface temperatures (Mutterlose et al., 2014; Bottini et al., 2015)
60 and a calcification crisis in calcareous nannoplankton known as the ‘nannoconid crisis’ (Erba,
61 1994). Despite its widespread extension and its recognition in numerous sedimentary basins
62 (Bréhéret, 1997; Bellanca et al., 2002; Ando et al., 2008; Vincent et al., 2010; Giraud et al.,
63 2018 among others) and shallow water carbonate platforms (Baudin et al., 1996; Luciani et
64 al., 2006; Najjarro et al., 2011; Graziano, 2013; Godet et al., 2014; Pictet et al., 2015; Amodio
65 and Weissert, 2017; Hueter et al., 2019), OAE1a has not yet been described in the Paris Basin
66 mainly because lower Aptian clayey deposits are poorly outcropping. In 2013, several
67 boreholes were drilled by Andra (the French National Radioactive Waste Management
68 Agency) to the south-east of the Paris Basin in order to characterise Aptian and Albian clayey
69 formations including Argiles à Plicatules, a so-called formation because of the occasional
70 occurrence of *Plicatula placunea* Lamarck, 1819, a common warm water bivalve (Squires and
71 Saul, 1997). One of these boreholes (AUB 121) intersected the Argiles à Plicatules Formation
72 with excellent recovery allowing detailed sedimentological, mineralogical and geochemical
73 studies to be performed; it also provided an opportunity to search for a record of OAE1a in
74 the Paris Basin. As a result, facies descriptions as well as mineralogical, Rock-Eval and
75 $\delta^{13}\text{C}_{\text{org}}$ analyses were performed to characterise the Aptian sediments deposited in the Paris

76 Basin. The main objectives were to precisely describe the whole succession of the Argiles à
77 Plicatules Formation, to highlight the record of OAE1a in the terrigenous shelf environment
78 of the Paris Basin and to specify climatic conditions, notably the fluctuations in the
79 hydrological cycle that prevailed during the Aptian through a high resolution study of the clay
80 minerals.

81

82 I - Geological context and biostratigraphy

83 The Paris Basin is a Meso-Cenozoic intracontinental basin that, today, is bordered by
84 Palaeozoic massifs including the Armorican Massif to the west, the Massif Central to the
85 south, the Vosges to the east and the Ardennes Massif to the north. During the Aptian, the
86 Paris Basin was occupied by a narrow epicontinental sea (strait) between the London-Brabant
87 Massif (LBM) and the Rhenish Massif (RM) to the north and a landmass comprising the
88 Armorican Massif (AM) and the Massif Central (MC) to the south (Fig. 1). This narrow
89 epicontinental sea, situated at a latitude comprised between 30 and 35°N, connected the
90 Tethys Ocean located to the south-east to the boreal realm toward the north-west (Masse et
91 al., 2000).

92 After a long period of continental evolution of the Paris Basin starting at the
93 Jurassic/Cretaceous transition (Purbeckian facies), transgressive marine sediments were
94 deposited above Early Cretaceous variegated continental and deltaic sediments, the so-called
95 Wealden facies (Allen, 1998; Guillocheau et al., 2000; Radley and Allen, 2012). To the south-
96 east of the Paris Basin, the Early Cretaceous continental sedimentation (Berriasian to
97 Barremian) was occasionally interrupted by the deposition of shallow marine sediments
98 including the early Hauterivian “Calcaires à Spatangues” Formation and the early Barremian
99 “Argiles Ostréennes” Formation, as a consequence of transgressions originating from the
100 south-east (Tethyan domain), whereas the late Barremian continental deposits consist of

101 variegated clays showing common root traces. From the Aptian, a continuous marine
102 sedimentation took place until the end of the Cretaceous.

103

104 I-1. Lithology of the AUB 121 borehole

105 The AUB 121 borehole is situated to the south-east of the Paris Basin, at Juzanvigny,
106 near Brienne le Château (Fig. 2). The lithological succession has been described in detail by
107 Amédéo et al. (2017). The 31 m-thick Argiles à Plicatules Formation is underlain by upper
108 Barremian continental deposits (Wealden facies) corresponding to weathering profiles
109 (laterite) and overlain by upper Aptian glauconitic sands corresponding to the “Sables Verts
110 de l’Aube” Formation (Fig. 3). Three distinct intervals (1 to 3) were defined within the
111 Argiles à Plicatules Formation:

- 112 - Unit 1, from 116.76 m to 111.90 m, includes black to grey clays with traces of
113 palaeosoils at the base. Woody debris and coalified compressions of pteridophytes
114 are common in this part of the formation (Fig. 4A). Some iron oolites-rich layers
115 (Fig. 4B) occasionally filling burrows occur at the base of this unit, while the top is
116 marked by the presence of prominent shelly beds (between 112.40 m and 111.90
117 m) (Fig. 4C).
- 118 - Unit 2, from 111.90 m to 106.30 m, consists of a grey-brown bioturbated
119 (*Chondrites*) clay, which appears to be homogeneous (no cycles can be
120 distinguished). Some *Plicatula* occur occasionally and ammonites are common in
121 the upper part of this unit.
- 122 - Unit 3, from 106.30 m to 86.10 m, corresponds to bioturbated khaki clays
123 (*Chondrites*) in which the cycles are clearly individualised and limited at the base
124 by bioturbated surfaces likely corresponding to firmgrounds. This poorly
125 fossiliferous unit shows scattered *Plicatula*, some oysters and ammonites which

126 allow a biostratigraphic division to be established. Coarser quartz grains and
127 glauconite occur at the topmost part of the formation announcing the overlying
128 sandy glauconitic sedimentation (Sables Verts de l'Aube Formation).

129

130 I-2. Biostratigraphy

131 Ammonites have been systematically collected along the core (Fig. 3). Although they
132 are not abundant, their study provides valuable information. A total of 19 ammonites were
133 found in the 30.66 m of the Argiles à Plicatules Formation recovered in borehole AUB 121, of
134 which 15 could be determined, at least at the generic level. They occur mostly as imprints in
135 clays, and in a few cases as internal moulds preserved either in the form of pyritic nuclei or
136 calcium phosphate nodules (Amédéo et al., 2017). All recognised taxa are cosmopolitan, with
137 a geographic distribution that includes the boreal, Tethyan and sometimes even southern
138 realms. This wide geographic distribution is explained by the fact that the summit of the early
139 Aptian corresponds to a high sea level (transgression of a second order eustatic cycle, see
140 Jacquin et al., 1998). The vertical distribution of the ammonites permits to establish a
141 biostratigraphic scheme.

142 The lower three meters of the Argiles à Plicatules Formation did not provide determinable
143 ammonites in the Juzanvigny boreholes and therefore the stratigraphic attribution of the
144 lowermost part of this formation remains uncertain. The occurrence of several *Roloboceras*
145 *transiens* Casey, 1961 in the neighbouring department of Yonne and *Megatyloceras* at the
146 base of the Argiles à Plicatules Formation (unpublished data) suggests that the interval could
147 be attributed to the *Deshayesites forbesi* Zone, as these ammonites are characteristic of this
148 biozone. The *Deshayesites deshayesi* Zone is undoubtedly recognised from 113.70 m to
149 105.15 m by the presence of an association including *Aconoceras (Aconoceras) nisoides*
150 Sarasin, 1893, *Pseudosaynella bicurvata* Michelin, 1838, *Deshayesites deshayesi* d'Orbigny,

151 1841 and *Lithancylus grandis* J. de C. Sowerby, 1828. The *Dufrenoyia furcata* Zone sensu
152 Reboulet compiler (2018) [= the *Tropaeum bowerbanki* Zone described by Casey (1961)] is
153 clearly identified from 102.50 m to 90.60 m by the occurrence of *Dufrenoyia cf. formosa*
154 Casey, 1964 and *Dufrenoyia cf. furcata* J. de C. Sowerby, 1836.

155

156 II – Analytical methods

157 II–1. Carbon stable isotopes, Total Organic Carbon and calcimetry

158 Organic carbon isotope compositions ($\delta^{13}\text{C}_{\text{org}}$) and Total Organic Carbon (TOC) were
159 measured on carbonate-free residues of 80 samples at the Biogéosciences Laboratory,
160 Université Bourgogne/Franche-Comté in Dijon. Sample powders were reacted with HCl (2N)
161 at room temperature for 24 h to remove the carbonate phases. Residues were rinsed with
162 deionised distilled water until neutral, centrifuged (4500 rpm for 15 min), and then dried at
163 50°C overnight. Aliquots of dried decarbonated samples (~7–50 mg) were then weighed in tin
164 capsules. TOC content and $\delta^{13}\text{C}_{\text{org}}$ measurements were performed at the Biogéosciences
165 Laboratory of the University of Bourgogne/Franche-Comté (Dijon, France) on a Vario
166 MICRO cube elemental analyzer (Elementar, Hanau, Germany) coupled in continuous flow
167 mode to an IsoPrime stable isotope ratio mass spectrometer (Isoprime, Manchester, UK).
168 USGS40 L-Glutamic acid (C = 40.8 wt%; $\delta^{13}\text{C}_{\text{VPDB}} = -26.39 \pm 0.04\text{‰}$) and IAEA-600
169 Caffeine ($\delta^{13}\text{C}_{\text{VPDB}} = -27.77 \pm 0.04\text{‰}$) certified reference materials were used for calibration.
170 The carbon isotopic composition is expressed in delta notation and reported in per mil (‰)
171 relative to the Vienna Pee Dee Belemnite (V-PDB) standard; the external reproducibility
172 based on duplicate analyses of the samples is better than $\pm 0.2\text{‰}$ (1σ).

173 The proportion of CaCO_3 is deduced by the difference in weight before and after
174 decarbonation.

175

176 II-2. Organic matter characterisation

177 A Rock-Eval 6 Turbo apparatus (Vinci Technologies) was used for the quantitative
178 and qualitative study of organic matter from 34 selected samples distributed over the entire
179 section. The method, described in detail by Lafargue et al. (1998) and Behar et al. (2001),
180 consists of a two-step analysis with programmed temperature: pyrolysis, under inert
181 atmosphere (N₂), followed by oxidation. Samples were analysed at the Institut des Sciences de
182 la Terre de Paris (UMR7193/Sorbonne Université). Crushed samples are first subjected to a 3
183 min isotherm at 300°C at which free hydrocarbons are volatilised (peak S1). Then, a heating
184 step with a ramp rate of 25°C/min leads to the vaporisation of products via the thermal
185 cracking of organic matter up to 650°C (peak S2). Pyrolysis effluents are continuously
186 detected by a flame ionisation detector (FID) and expressed in mg per g of sample. Organic
187 CO and CO₂ are measured online as well by an infrared cell (peak S3). At the end of the
188 pyrolysis step, samples are automatically transferred into an oxidation oven where they are
189 subjected to a 1 min isotherm at 300°C then a ramp rate of 20°C/min up to 850°C. The total
190 signals of both organic and mineral CO and CO₂ are expressed in mg per g of samples. All
191 these parameters can be used to calculate the TOC content. The hydrogen index (HI),
192 corresponding to the quantity of hydrocarbon compounds released during pyrolysis relative to
193 the TOC (S2/TOC) in mg of HC per g of TOC as well as the oxygen index (OI)
194 corresponding to the organic CO₂ released during pyrolysis relative to the TOC (S3/TOC) in
195 mg of CO₂ per g of TOC are also calculated. HI and OI are correlated to the H/C and O/C
196 atomic ratios respectively, which can be used to determine the origin of the organic matter.
197 T_{max} is defined as the pyrolysis temperature at which the maximum amount of hydrocarbon is
198 yielded by kerogen (Espitalié et al., 1977). T_{max} increases linearly with the maturation degree
199 of the organic matter, thus giving a rapid estimate of the thermal maturity of sedimentary
200 basins (Espitalié, 1986).

201

202 II-3. Clay mineralogy

203 A total of 80 samples were analysed using X-Ray Diffraction (XRD). After moderate
204 grinding in a mortar, powdered samples were decarbonated with a 0.2N HCl solution. The
205 < 2 μm fraction (clay-sized particles) was extracted with a syringe after deflocculation and
206 decantation of the suspension for 95 minutes following Stokes' law; this fraction was then
207 centrifuged. Clay residue was then smeared on oriented glass slides and run in a Bruker D8
208 diffractometer with $\text{CuK}\alpha$ radiations, a LynxEye detector and a Ni filter with a voltage of 40
209 kV and an intensity of 25 mA (Biogéosciences laboratory, Université Bourgogne/Franche-
210 Comté in Dijon, France). Goniometer scanning ranged from 2.5° to 28° for each analysis.
211 Three runs were performed for each sample to discriminate the clay phases: 1) air-drying; 2)
212 ethylene-glycol solvation at room temperature during 24 hours; and 3) heating at 490°C
213 during 2 hours, as recommended by Moore and Reynolds (1997). Clay minerals were
214 identified using their main diffraction (d_{001}) peaks and by comparing the three diffractograms
215 obtained. The relative proportions of the clay minerals are estimated using peak intensity
216 ratios. The error margin of the method is approximately $\pm 5\%$.

217

218 III – Results

219 III-1. CaCO_3 , Organic matter characterisation and $\delta^{13}\text{C}_{\text{org}}$

220 In the Argiles à Plicatules Formation, the proportion of CaCO_3 is very low (around
221 3%) in all of the samples studied (Fig. 5). The total organic carbon (TOC) content measured
222 on the 34 selected samples using Rock-Eval pyrolysis is also very low, comprised between
223 0.1 and 0.52% (Table 1). As the quantity of organic matter (OM) is low, the Rock-Eval
224 parameters are only partly reliable. However, some reliable T_{max} values lower than 420°C
225 indicate that OM is immature (below the oil window). Organic matter is more abundant in

226 lithological unit 1 at the base of the section; this was expected since macroscopic woody
227 debris and fern pinnules preserved as coalified compressions were observed (Fig. 4B).

228 The $\%C_{org}$ obtained after isotopic analyses is between 0.15 and 0.82 (Fig. 4),
229 systematically showing slightly higher values than those obtained using Rock-Eval pyrolysis,
230 but with the same trends. Higher values are recorded at the base of the core in lithological unit
231 1 which is enriched in continental organic matter. By comparison with unit 3, a slight increase
232 is recorded in the interval corresponding approximately to lithological unit 2 (Fig. 5);
233 however, significant enrichment in marine organic matter, which would have indicated it was
234 preserved in a significantly oxygen-depleted environment, is not recorded.

235 The $\delta^{13}C_{org}$ values fluctuate between -24.19‰ and -27.91‰ (Fig. 4). A prominent
236 negative excursion is recorded between 112 and 110 m at the base of lithological unit 2,
237 followed by a shift to higher (close to -25‰) and relatively constant values up-section.

238

239 III-2. Clay mineralogy

240 The following main clay minerals were identified: a R0 type illite-smectite mixed-
241 layer (17 Å based on a glycolated run condition) referred to as smectite for the following
242 sections; chlorite (14.2 Å, 7.1 Å, 4.7 Å and 3.54 Å peaks); illite (10 Å, 5 Å, 3.33 Å peaks);
243 kaolinite (7.18 Å and 3.58 Å peaks) and vermiculite (14 Å in air-drying conditions, 14.5-15 Å
244 after ethylene-glycol solvation and 10 Å peaks after heating). In addition, traces of
245 pyrophyllite are occasionally suspected by the occurrence of a small peak at 9.3 Å. The clay
246 mineral assemblages are predominantly composed of illite generally between 40 and 50% and
247 kaolinite with proportions comprised between 20 and 45%. Minor amounts of chlorite (less
248 than 10%), vermiculite (around 10%) and smectite (generally less than 10%, except at the top
249 of the formation where the proportions of this mineral may reach 50%) are associated with
250 these two clay species (Fig. 6). Traces of pyrophyllite are only identified at the base of the

251 core. Four stratigraphic intervals can be distinguished according to the clay mineralogy.
252 Interval 1 corresponds to the lowermost part of the formation below the bioclastic
253 accumulation and coincides with lithological unit 1. In this interval, the proportion of
254 vermiculite is relatively high and decreases up-section while the proportion of illite increases.
255 The second interval, from 112 to 104.5 m is characterised by the relative abundance of
256 kaolinite (30 to 45%) notably at the base of this interval where the proportions of this mineral
257 show a maximum (45%), and by the absence of smectite. The third interval from 104.5 m to
258 87.5 m shows a monotonous clay assemblage without any significant change and is composed
259 of approximately 5% of chlorite, 45% of illite, 10% of vermiculite, 10% of smectite and 30%
260 of kaolinite. The uppermost part of the formation (interval 4) shows a sharp increase in the
261 proportions of smectite balanced by significant decreasing proportions of illite and kaolinite.

262

263 IV - Discussion

264 IV-1. Depositional environments of the Argiles à Plicatules Formation

265 The lowermost part of the formation overlying the continental Wealden facies and
266 consisting of dark grey clays with abundant iron oolites (Fig. 4A) and common terrestrial
267 plant remains (woods and foliar remains, Fig. 4B) likely corresponds to transgressive
268 sediments deposited in coastal environments. Similar facies were described in boreholes
269 drilled close to Soulaines to the east of Juzanvigny (Fig. 2) where transgressive facies are
270 clearly separated by emersion features suggesting, several transgressive events at the
271 beginning of the Aptian transgression (Ferry, 2000). Foliar meso- and macro-remains
272 exclusively consist of fragments of pinnae and isolated fern pinnules preserved as coalified
273 compressions (Fig. 4B). The largest pinna fragment is 22 mm long. The pinnae bear up to 8
274 mm long and 3 mm wide alternate to subopposite, oblong, thick and leathery pinnules. They
275 are attached by a broad base to the rachis and display a rounded apex and an entire margin.

276 Sometimes the pinnules are slightly inclined forward. The midrib is straight and ends before
277 the apex of the pinnule. These features as well as the reticulate veins allow to ascribe these
278 specimens to *Weichselia reticulata* (Stokes and Webb) Fontaine which is a common fern in
279 the Early Cretaceous flora from Europe (Blanco-Moreno et al., 2018). In France, *W. reticulata*
280 was previously reported from the Wealden facies of the Nord department (Carpentier, 1927)
281 and the Oise department (Carpentier, 1929). The abundance of plant remains in oolitic facies
282 shows that the depositional environment was influenced by strong terrestrial inputs. Although
283 *Weichselia* mostly occurred in a continental environment in Europe (Blanco-Moreno et al.,
284 2018), this report shows that *W. reticulata* was one of the components of littoral flora during
285 the earliest Aptian.

286 As they occur immediately above the upper Barremian lateritic palaeo-alteration, iron
287 oolites may be reworked from the lateritic soils (Bhattacharyya, 1983). However, iron oolites
288 may also have formed as a replacement of a pre-existing ooid structure or via the precipitation
289 of an iron aluminosilicate (chamosite/berthierine) grain in shallow marine environments
290 (Velde, 1989). Iron may be provided in the sedimentary environment by the weathering of the
291 proximal continental areas. In most cases iron oolites are associated with transgressive
292 deposits, which is the case in the lowermost part of the Argiles à Plicatules Formation, and are
293 indicators of condensed sections (Collin et al., 2005; Clement et al., 2020).

294 Up-section, the deposits increasingly less silty show common bivalves. The first
295 ammonite occurs at 113.70 m indicating open-marine environments. The prominent shell
296 horizon intercalated in the clayey succession at the top of lithological unit 1 between 112.40
297 m and 111.90 m (Fig. 4C) can be divided into two parts. The first corresponds to a bed
298 comprising pluri-centimetric bivalve shells forming the base of a 30 cm-thick fining up
299 sequence. The top of this bed, which is 112.05 m (Fig. 4C), is bioturbated. Above, a second
300 accumulation of bivalves is associated with centimetric clasts. The succession may

301 correspond to two successive storm deposits separated by a bioturbated surface. This suggests
302 a deposition above storm wave base in upper offshore environments and a deepening trend of
303 the basin as a consequence of the Aptian transgression. This trend continues up-section from
304 111.90 m to 106.30 m, as the homogenous faintly bioturbated clays without any sedimentary
305 structure suggest a deposition in a quiet environment, below the storm wave base (lower
306 offshore). Rare calcareous nannofossils observed in smear slides occur in most of the samples
307 and are likely responsible for the carbonate content (close to 3%) of the sediment. From
308 106.30 m to the top of the formation, the clays contain more silt. Bioturbated surfaces indicate
309 sedimentation breaks that are consistent with the common occurrence of phosphate
310 (carbonate-apatite) nodules.

311 The Argiles à Plicatules Formation encompasses a transgressive interval from the base
312 to a maximum flooding surface located in the interval between 111.90 m and 106.30 m. The
313 uppermost 20 m of the formation corresponds to a highstand system tract terminated by a
314 prominent bioturbated surface between the Argiles à Plicatules and the Sables Verts de l'Aube
315 formations deposited at a shallower water depth in shoreface environments.

316

317 IV-2. Evolution of the $\delta^{13}\text{C}_{\text{org}}$ and organic matter contents

318 Several of the isotopic segments initially distinguished by Menegatti et al. (1998)
319 across the "Livello Selli", which includes OAE1a, or its equivalent in the Tethys Ocean, and
320 which were subsequently recognised worldwide and used as a reliable tool for
321 chemostratigraphic correlations, are clearly identified in the studied borehole: C2 at the base
322 of the section, C3 corresponding to the negative excursion showing the lowest values of
323 $\delta^{13}\text{C}_{\text{org}}$ between 111.80 and 110 m, C4, C5 and C6 characterised by a shift to higher values
324 and finally C7 (Fig. 5).

325 The ‰ negative excursion that occurs immediately before OAE1a and corresponding
326 to the C3 segment is clearly identified. It occurs probably in the *deshayesi* Zone just above the
327 bioclastic accumulations interpreted as storm deposits, with an amplitude comparable to that
328 observed in many sedimentary basins (Menegatti et al., 1998; Ando et al., 2008). The C3
329 segment is relatively thick (1.80 m) indicating a relatively high sedimentation rate and shows
330 two distinct negative excursions separated by a positive excursion with a small amplitude,
331 which can also be observed in the $\delta^{13}\text{C}_{\text{carb}}$ curves from sections from south-east France (Kuhnt
332 et al., 1998; 2011). This may suggest the existence of, at least, two successive volcanic CO₂
333 pulses at the origin of the emplacement of the Ontong Java-Manihiki-Hikurangi Plateau
334 (Lorenzen et al., 2013; Naafs et al., 2016).

335 Surprisingly, the interval corresponding to the $\delta^{13}\text{C}_{\text{org}}$ positive excursion is not
336 significantly enriched in organic matter and the facies of the Argiles à Plicatules Formation
337 are extremely homogeneous, unchanged in colour and without any laminations. The absence
338 of significant organic matter enrichment is surprising since the deep, quiet lower offshore
339 depositional environment was favourable to the preservation of marine organic matter. Some
340 authors report an absence of significant marine organic matter enrichment in several
341 sedimentary basins of northern Spain including the Basco-Cantabric Basin (Garcia-Mondejar
342 et al., 2015) and the Organyà Basin (Sanchez-Hernandez and Maurasse, 2016) although they
343 correspond to oxygen-depleted environments but without prolonged anoxia.

344 In the Paris Basin, the absence of OM enrichment can be explained in several ways.

345 1) The primary productivity was probably low as suggested by the very low carbonate
346 content of the succession. The carbonate fraction of the Argiles à Plicatules Formation, which
347 does not exceed 4%, is composed of rare nannofossils including the genus *Watznaueria*,
348 *Zeugrhabdotus*, *Rhagodiscus*, *Biscutum*, *Discorhabdus* and *Cyclagelosphaera* (F. Giraud, *in*

349 Ferry, 2000). The scarcity of fauna and flora suggests that the environment must have been
350 oligotrophic.

351 2) The absence of anoxia in the Aptian sea-way between the LBM/RM and the
352 AM/MC (Fig. 1) may be also explained by the presence of marine currents flowing through
353 the strait thus favouring relatively well-oxygenated environments. However, except the
354 occasional occurrence of phosphate nodules that may indicate low sedimentation rate due to
355 the winnowing of fine particles, there is no evidence of hydrodynamic influences expressed in
356 the sedimentary facies.

357 3) The oxygen-minimum zone that was clearly expressed in the Tethys Ocean was
358 deeper and did not reach the relatively shallow environments of the Paris Basin. This is
359 plausible, given that Coccioni et al. (1987) and Westermann et al. (2013) show that anoxic to
360 euxinic conditions developed in the deeper part of the Tethys Ocean during OAE 1a, while
361 conditions were not as reducing in shallower environments.

362 By comparison with several sections from the Tethys ocean, the $\delta^{13}\text{C}_{\text{org}}$ positive
363 excursion is less pronounced than expected, what could be the result of several gaps coeval
364 with the positive excursion like those observed in carbonate platform environments (Wissler
365 et al., 2005). However, except the occurrence of bioturbated surfaces and some scattered
366 phosphate nodules, there is no clear evidence of significant sedimentation breaks.

367

368 IV-3. Significance of clay mineral assemblages

369 IV-3-1. Diagenetic influences

370 Before examining the significance of clay mineral assemblages in terms of the
371 palaeoclimate and palaeoenvironment, it is essential to ensure that they are predominantly
372 detrital in origin without any significant influence of burial diagenesis, thermal influences or
373 authigenic growth during early or late diagenesis. The post-Aptian sedimentary successions

374 probably never exceeded 1100 m (Robaszynski et al., 2005), which is consistent with a weak
375 thermal impact (Torelli et al., 2020) compatible with the occurrence of smectite and immature
376 organic matter. Consequently, it is unlikely that clay minerals may have been transformed
377 during burial diagenesis. This conclusion is consistent with many studies performed to the
378 east of the Paris Basin on upper Jurassic deposits showing that the thermal influences remain
379 very weak even when these deposits are more deeply buried (Pellenard et al., 1999; Pellenard
380 and Deconinck, 2006; Blaise et al., 2014; Mangenot et al., 2018).

381 Small quantities of glauconite commonly occur in the uppermost part of the Argiles à
382 Plicatules Formation at the transition with the overlying Sables verts de l'Aube Formation.
383 Glauconite is an iron-rich illite and the granules are coarser than the clay fraction and
384 normally not included in the clay fraction. However, as the samples are ground in preparation
385 for XRD analyses, it is possible that glauconite was partly introduced in the clay fraction and
386 slightly increases the total proportion of illite at the top of the formation.

387

388 Therefore, we assume that most clay minerals are detrital in origin and may be useful
389 to precise environmental conditions that prevailed during the early Aptian around the Paris
390 Basin.

391

392 IV-3-2. Environmental control of the clay sedimentation

393 Primary minerals, including illite, chlorite and pyrophyllite constitute more than half
394 of the clay fraction. The abundance of these minerals suggests a relatively intense erosion on
395 the continental areas bordering the Paris Basin. Although clay minerals may be transported
396 over long distances, they likely originated from the Palaeozoic massifs surrounding the Paris
397 Basin. Illite, chlorite and pyrophyllite originated from the erosion of igneous and
398 metamorphic rocks from the AM/MC and from the low grade metamorphic rocks from the

399 LBM. Vermiculite is also common, notably at the base of the formation. This mineral also
400 occurs in lower to middle Albian clayey strata of the Paris Basin and likely originated from
401 the north, i.e. from the LBM (Gale et al., 1996; Corentin et al., 2020). Vermiculitic clays
402 corresponding to illite/vermiculite mixed-layers were also identified together with illite and
403 kaolinite in the Aptian deposits of the Lower Saxony Basin of Germany (Benesch et al., 1998)
404 and likely originate from the moderate weathering of chlorite.

405 Kaolinite is also abundant with maximum values in interval 2 characterised by the
406 homogeneous clay deposited in the deepest environments. Therefore, in the present case, the
407 abundance of kaolinite cannot be a consequence of its preferential deposition in nearshore
408 environments as suggested by Godet et al., (2008). The stratigraphic interval coinciding with
409 the $\delta^{13}\text{C}_{\text{org}}$ negative excursion is strongly depleted in smectite suggesting that a particularly
410 hydrolysing (warm and humid) climate was established at that time (Chamley, 1989; Ruffell
411 et al., 2002). By contrast, in the topmost part of the Argiles à Plicatules Formation, the
412 decreasing proportions of kaolinite balanced by increasing proportions of smectites suggest
413 increasingly arid climate conditions confirming a certain variability in the Aptian climate
414 (Dumitrescu et al., 2006; Bottini et al., 2015; Naafs and Pancost, 2016). These arid climatic
415 conditions also seem to have prevailed during the Aptian-Albian in the Algarve Basin
416 (Southern Portugal) where sedimentary rocks are depleted in kaolinite and show a high
417 amount of the xerophytic pollen *Classopollis* (Heimhofer et al., 2008). Aridity may be a
418 consequence of colder climate (cold snaps) recorded at the Aptian/Albian transition
419 (Mutterlose et al., 2009; Maurer et al., 2012; Millán et al., 2014).

420

421 IV.4. Climate evolution during the deposition of the Argiles à Plicatules Formation

422 A comparison of $\delta^{13}\text{C}_{\text{org}}$ and the mineralogical data shows that the C3 segment
423 corresponding to the negative excursion recorded prior to the OAE1a is characterised by an

424 increase in the proportions of kaolinite (Fig. 7) at the same time as a decrease in the
425 proportions of smectites. This suggests the installation of a more humid climate as a
426 consequence of an acceleration of the hydrological cycle induced by the warming triggered by
427 the increase in pCO₂ (Keller et al., 2011; Bodin et al., 2015; Naafs and Pancost, 2016). There
428 are several lines of evidence for such a climatic change. Wortmann et al. (2004) suggested
429 that the widespread occurrence of sandstones in the Tethys-Atlantic seaway was a
430 consequence of increasing erosion rates due to the acceleration of the hydrological cycle in
431 the wake of the early Aptian carbon cycle perturbation. Increasing global weathering intensity
432 coeval with OAE1a is also suggested by calcium isotopes (Blättler et al., 2011) measured in
433 carbonate deposits from several areas including southern England, Italy and Resolution Guyot
434 from the mid-pacific mountains. Hochuli et al. (1999) also describe global warming resulting
435 in increasing riverine fluxes. The warming is evidenced by a drop in δ¹⁸O, TEX₈₆ data and by
436 pollen records. The δ¹⁸O data from many sedimentary basins including the South Pacific
437 shows, that the ocean waters warmed strongly during the negative excursion and that
438 temperatures then decreased probably due to the storage of organic matter in the sediments
439 (Ando et al., 2008; Stein et al., 2011; Zakharov et al., 2013). These observations are in
440 agreement with the maximum proportions of kaolinite and the decrease in the proportion of
441 *Classopollis*, (xerophytic pollen) in the Maestrat Basin (eastern Spain) during OAE1a (Cors et
442 al. 2015). Tex₈₆ data obtained in the Selli level (or other equivalents of the OAE1a) also
443 indicate particularly warm sea-surface temperatures (Schouten et al., 2003; Dumitrescu and
444 Brassel, 2006; Mutterlose et al., 2010, 2014).

445 The global warming that occurred prior to OAE1a is therefore likely responsible for an
446 acceleration of the hydrological cycle and for the increase of kaolinite because of increasing
447 runoff and hydrolyses on the continental areas bordering the Paris Basin. The high
448 proportions of kaolinite in Aptian deposits of the Paris Basin could be explained by the

449 formation of kaolinite in soils, but the duration of the climatic perturbation is relatively short,
450 between 280 and 350 kyr (Lorenzen et al., 2013), while the formation of kaolinite in soils
451 required a longer time estimated at least to 1 myr (Thiry, 2000). It is more likely that kaolinite
452 was principally reworked from kaolinite-rich weathering profiles developed over the
453 Palaeozoic massifs during the Early Cretaceous (Jurassic-Cretaceous transition to Barremian)
454 (Meyer, 1976; Gilg, 2000; Quesnel, 2003; Yans, 2003; Thiry et al., 2005, 2006; Corentin et
455 al., 2020). As detrital clays including kaolinite may be reworked from older rocks or from
456 palaeo-alterations, their climatic significance may be questioned (Jeans et al., 2001), but
457 overall, illite and kaolinite dominated clay assemblages of the Aptian in the Paris Basin point
458 to a significant runoff and consequently to humid climate conditions. It is probable, that
459 fluctuations in the hydrological cycle controlling fluvial inputs occurred before and during
460 OAE1a as evidenced by changing environmental conditions in terms of anoxia/dysoxia
461 (Socorro and Maurasse, 2018; 2020).

462 Although the reliability of $\delta^{18}\text{O}$ data has recently been confirmed (O'Brien et al.,
463 2017), the acceleration of the hydrological cycle following the very hot episode preceding
464 OAE1a can be used to address the question of the significance of the low $\delta^{18}\text{O}$ values
465 recorded prior to OAE1a. $\delta^{18}\text{O}$ -values may also be a result of a slight decrease in ocean
466 salinity. This question, already addressed for other periods, shows that it is essential to take
467 better account of the fluctuations in the hydrological cycle in the context of climatic
468 reconstructions. In addition, higher runoff may increase thermohaline stratification that may
469 be involved in the development of an OAE (e.g. Erbacher et al., 2001; Van Helmond et al.,
470 2015).

471

472 Conclusions

473 For the first time, OAE1a is clearly identified in argillaceous deposits, the so-called
474 Argiles à Plicatules Formation, deposited in the Paris Basin. Most of the C-isotope segments
475 defining the OAE 1a interval are identified in the stratigraphic succession. However, the
476 section is devoid of any significant marine organic matter enrichment likely because the
477 Tethyan oxygen-depleted deep-water masses did not reach the epicontinental areas of the
478 Paris Basin. The global warming preceding OAE1a is likely responsible for an acceleration of
479 the hydrological cycle, an increase in runoff and the reworking of kaolinite from
480 palaeoweathering profiles cropping out on the Palaeozoic massifs bordering the Paris Basin.
481 As indicators for an acceleration of the hydrological cycle are also recorded in other areas, a
482 slight decrease in ocean salinity prior to OAE1a may be responsible in part for its
483 development and questions the reliability of the sea surface temperature deduced from the
484 $\delta^{18}\text{O}$ values. The hydrolysing conditions were so intense prior to and during OAE1a that
485 smectite totally disappeared from the clay fraction. However, smectite increases in the upper
486 part of the succession suggesting, that more arid conditions prevailed at that time possibly in
487 relation with a colder climate during the Aptian/Albian transition. The changing clay mineral
488 assemblages suggest, that the Aptian stage was characterised by a climate instability marked
489 not only by changes in temperature but also in the hydrological cycle.

490

491 Acknowledgements: We would like to thank Claude Aurière, who is in charge of storing
492 Andra's cores, for his help in studying the boreholes. We would like to warmly thank the two
493 reviewers, Jochen Erbacher and Helmut Weissert for their constructive and helpful comments
494 on the initial version of the manuscript.

495

496 References

497

498 Allen, P., 1998. Purbeck-Wealden (early Cretaceous) climates. Proceedings of the Geologists'
499 Association 109, 197–236.

500 Amédro, F., Matrimon, B., Deconinck, J.F., Huret, E. Landrein, P., 2017. Les forages de
501 Juzanvigny (Aube, France) : litho-biostratigraphie des formations du Barrémien à
502 l'Albien moyen dans l'est du bassin de Paris et datations par les ammonites.
503 Geodiversitas 39, 2, 185-212.

504 Amodio, S., Weissert, H., 2017. Palaeoenvironment and palaeoecology before and at the onset
505 of Oceanic Anoxic Event (OAE)1a: Reconstructions from Central Tethyan archives.
506 Palaeogeography, Palaeoclimatology, Palaeoecology 479, 71–89.

507 Ando, A., Kaiho, K., Kawahata, H., Kakegawa, T., 2008. Timing and magnitude of early
508 Aptian extreme warming: Unraveling primary $\delta^{18}\text{O}$ variation in indurated pelagic
509 carbonates at Deep Sea Drilling Project Site 463, central Pacific Ocean.
510 Palaeogeography, Palaeoclimatology, Palaeoecology 260, 463–476.

511 Baudin, F., 1996. Enregistrement de l'événement anoxique aptien inférieur dans les faciès
512 péritidaux du Guyot Resolution (océan Pacifique Nord-Ouest). C.R Acad. Sci., Paris
513 323 (IIa), 221-228.

514 Behar, F., Beaumont, V., De B. Penteado, H.L., 2001. Technologie Rock-Eval 6 :
515 performances et développements. Oil and Gas Science and Technology, Revue de
516 l'Institut Français du Pétrole 56, 111–134.

517 Bellanca, A., Erba, E., Neri, R., Premoli Silva, I., Sprovieri, M., Tremolada, F., Verga, D.,
518 2002. Palaeoceanographic significance of the Tethyan "Livello Selli" (early Aptian)
519 from the Hybla Formation, northwestern Sicily: biostratigraphy and high-resolution
520 chemostratigraphic records. Palaeogeography, Palaeoclimatology, Palaeoecology 185,
521 175–196.

522 Benesch, M., Heydemann, A., Usdowski, E., 1998. Mineralogy of the Lower Aptian
523 sediments from the borehole Hoheneggelsen KB 40, with special emphasis on the clay
524 mineralogy. *Cretaceous Research* 19, 569-580.

525 Blaise, T., Barbarand, J., Kars, M., Ploquin, F., Aubourg, C., Brigaud, B., Cathelineau, M., El
526 Albani, A., Gautheron, C., Izart, A., Janots, D., Michels, R., Pagel, M., Pozzi, J.P.,
527 Boiron, M.C., Landrein, P., 2014. Reconstruction of low temperature (<100° C) burial
528 in sedimentary basins: A comparison of geothermometer in the intracontinental Paris
529 Basin. *Marine and Petroleum Geology* 53, 71-87.

530 Blanco-Moreno, C., Gomez, B., Buscalioni, Á., 2018. Palaeobiogeographic and metric
531 analysis of the Mesozoic fern *Weichselia*. *Geobios* 51(6), 571-578.

532 Blättler, C.L., Jenkyns, H.C., Reynard, L.M., Henderson, G.M., 2011. Significant increases in
533 global weathering during Oceanic Anoxic Events 1a and 2 indicated by calcium
534 isotopes. *Earth and Planetary Science Letters* 309, 77–88

535 Bodin, S., Meissner, P., Janssen, N.M.M., Steuber, T., Mutterlose, J., 2015. Large igneous
536 provinces and organic carbon burial: Controls on global temperature and continental
537 weathering during the Early Cretaceous. *Global and Planetary Change* 133, 238–253.

538 Bottini, C., Cohen, A.S., Erba, E., Jenkyns, H.C., Coe, A.L., 2012. Osmium-isotope evidence
539 for volcanism, weathering, and ocean mixing during the early Aptian OAE 1a.
540 *Geology* 40, 583–586.

541 Bottini, C., Erba, E., Tiraboschi, D., Jenkyns, H.C., Schouten, S., Sinninghe Damsté, J.S.,
542 2015. Climate variability and ocean fertility during the Aptian Stage. *Climate of the*
543 *Past* 11, 383-402.

544 Bréhéret, J.G., 1997. L’Aptien et l’Albien de la Fosse vocontienne (des bordures au bassin).
545 Évolution de la sédimentation et enseignements sur les événements anoxiques. Société
546 Géologique du Nord, Publ. n° 25, 644 p.

- 547 Carpentier, A., 1927. La flore wealdienne de Féron-Glageon (Nord). Mémoires de la Société
548 Géologique du Nord 1, 1–151.
- 549 Carpentier, A., 1929. Recherches sur les végétaux fossiles des argiles éocéniques du Pays
550 de Bray. Bulletin de la Société Géologique de France 4(29), 89-96.
- 551 Casey, R., 1961. The stratigraphical paleontology of the Lower Greensand. Palaeontology,
552 London 3, 487-621, pl. 77-84.
- 553 Chamley, H., 1989. Clay sedimentology. Springer, Berlin, Heidelberg, 623 p.
- 554 Charbonnier, G., Föllmi, K.G., 2017. Mercury enrichments in lower Aptian sediments support
555 the link between Ontong Java large igneous province activity and oceanic anoxic
556 episode 1a. Geology 45, 1, 63-66.
- 557 Clement, A.M., Tackett, L.S., Ritterbush, K.A., Ibarra, Y., 2020. Formation and stratigraphic
558 facies distribution of early Jurassic iron oolite deposits from west central Nevada,
559 USA. Sedimentary Geology 395, 105537.
- 560 Coccioni, R., Erba, E., Premoli Silva, I., 1992. Barremian-Aptian calcareous plankton
561 biostratigraphy from the Gorgo a Cerbara section (Marche, Central Italy) and
562 implication for planktonic evolution. Cretaceous Research 13, 517-537.
- 563 Coccioni, R., Nesci, O., Tramontana, M., Wezel, F.C., Moretti, E., 1987. Descrizione di un
564 livello guida “radiolaritico-bituminoso-ittiolitico” alla base delle Marne a Fucoidi
565 nell’Appennino Umbrio-Marchigiano. Bollettino della Società geologica italiana 106,
566 1, 183-192.
- 567 Collin, P., Loreau, J., Courville, P., 2005. Depositional environments and iron ooid formation
568 in condensed sections (Callovian–Oxfordian, south-eastern Paris basin, France).
569 Sedimentology 52, 969–985.

570 Cors, J., Heimhofer, U., Adatte, T., Hochuli, P.A., Huck, S., Bover-Arnal, T., 2015. Climatic
571 evolution across oceanic anoxic event 1a derived from terrestrial palynology and clay
572 minerals (Maestrat Basin, Spain). *Geological Magazine* 152, (4), 632–647.

573 Corentin, P., Deconinck, J.F., Pellenard, P., Amédéo, F., Bruneau, L., Chenot, E., Matrimon, B.,
574 Huret, E., Landrein, P., 2020. Environmental and climatic controls of the clay
575 mineralogy of Albian deposits in the Paris and Vocontian basins (France). *Cretaceous*
576 *Research* 108, <https://doi.org/10.1016/j.cretres.2019.10434>.

577 Dumitrescu, M., Brassell, S.C., 2006. Compositional and isotopic characteristics of organic
578 matter for the Early Aptian Oceanic Anoxic Event at Shatsky Rise, ODP Leg 198.
579 *Palaeogeography, Palaeoclimatology, Palaeoecology* 235, 168–191.

580 Dumitrescu, M., Brassell, S.C., Schouten, S., Hopmans, E.C., Sinninghe Damsté, J.S., 2006.
581 Instability in tropical Pacific sea-surface temperatures during the early Aptian.
582 *Geology* 34, 10, 833–836.

583 Erba, E., 1994. Nannofossils and superplumes: the early Aptian “nannoconid crisis”.
584 *Paleoceanography* 9, 483–501.

585 Erba, E., 2004. Calcareous nannofossils and Mesozoic oceanic anoxic events. *Marine*.
586 *Micropaleontology* 52, 85–106.

587 Erba, E., Duncan, R.A., Bottini, C., Tiraboschi, D., Weissert, H., Jenkyns, H.C., Malinverno,
588 A., 2015. Environmental consequences of Ontong Java Plateau and Kerguelen Plateau
589 volcanism. In *Geological Society of America Special Papers*, Vol. 511. Geological
590 Society of America, 271–303 pp.

591 Erbacher, J., Thürow, J., Littke, R., 1996. Evolution patterns of radiolarian and organic matter
592 variations: a new approach to identify sea-level changes in mid-Cretaceous pelagic
593 environments. *Geology* 24, 499–502.

594 Erbacher, J., Huber, B. T., Norris, R. D., Markey, M., 2001. Increased thermohaline
595 stratification as a possible cause for an ocean anoxic event in the Cretaceous period.
596 *Nature* 409, 325–327.

597 Espitalié, J., 1986. Use of Tmax as a maturation index for different types of organic matter.
598 Comparison with vitrinite reflectance. In: *Thermal Modelling in Sedimentary Basins*.
599 Technip, Paris, pp. 475–496.

600 Espitalié, J., La Porte, J.L., Madec, M., Marquis, F., Le Plat, P., Paulet, J., Boutefeu, A., 1977.
601 Rapid method for source rocks characterization and for determination of petroleum
602 potential and degree of evolution. *Oil and Gas Science and Technology, Revue de*
603 *l’Institut Français du Pétrole* 32, 23–42.

604 Ferry, S., 2000. Analyse sédimentologique de la série albo-aptienne de Soulaines – Projet site
605 TFA. Unpublished report n° F RP O UCB TFA 00-204/A, Andra, 62 p.

606 Föllmi, K.B., 2012. Early Cretaceous life, climate and anoxia. *Cretaceous Research* 35, 230-
607 257.

608 Gale, A.S., Huggett, J.M., Gill, M., 1996. The stratigraphy and petrography of the Gault Clay
609 Formation (Albian, Cretaceous) at Redcliff, Isle of Wight. *Proceedings of the*
610 *Geologists' Association* 107, 287-298.

611 Garcia-Mondejar, J., Fernandez-Mendiola, P.A., Owen, H.G., 2015. The OAE1a in Cuchia
612 (Early Aptian, Spain): C and O geochemistry and global correlation. *Acta Geologica*
613 *Polonica* 65, (4), 525–543.

614 Gilg, A. 2000. D–H evidence for the timing of kaolinization in Northeast Bavaria, Germany.
615 *Chemical geology* 170, 5 – 18.

616 Giraud, F., Pittet, B., Grosheny, D., Baudin, F., Lécuyer, C., Sakamoto, T., 2018. The
617 palaeoceanographic crisis of the Early Aptian (OAE 1a) in the Vocontian Basin (SE
618 France). *Palaeogeography, Palaeoclimatology, Palaeoecology* 511, 483–505.

619 Godet, A., Bodin, S., Adatte, T., Föllmi, K.B., 2008. Platform-induced clay-mineral
620 fractionation along a northern Tethyan basin-platform transect: implications for the
621 interpretation of Early Cretaceous climate change (Late Hauterivian-Early Aptian).
622 *Cretaceous Research* 29, 830–847.

623 Godet, A., Hfaiedh, A., Arnaud-Vanneau, A., Zghal, I., Arnaud, H., Ouali, J., 2014. Aptian
624 palaeoclimates and identification of an OAE1a equivalent in shallow marine
625 environments of the southern Tethyan margin: Evidence from Southern Tunisia (Bir
626 Oum Ali section, Northern Chott Chain). *Cretaceous Research* 48, 110-129.

627 Graziano, R., 2013. Sedimentology, biostratigraphy and event stratigraphy of the Early Aptian
628 Oceanic Anoxic Event (OAE1A) in the Apulia Carbonate Platform Margin - Ionian
629 Basin System (Gargano Promontory, southern Italy). *Cretaceous Research* 39, 78-111.

630 Guillocheau, F., Robin, C., Allemand, P., Bourquin, S., Brault, N., Dromart, G., Friedenber,
631 R., Garcia, J.-P., Gaulier, J.-M., Gaumet, F., Grosdoy, B., Hanot, F., Le Strat, P.,
632 Mettraux, M., Nalpas, T., Prijac, C., Rigollet, C., Serrano, O., Granjean, G., 2000.
633 Meso-Cenozoic geodynamic evolution of the Paris Basin: 3D stratigraphic constraints.
634 *Geodinamica Acta*, 13, 189–245.

635 Heimhofer, U., Adatte, T., Hochuli, P.A., Burla, S., Weissert, H., 2008. Coastal sediments
636 from the Algarve: low-latitude climate archive for the Aptian-Albian. *International*
637 *Journal of Earth Sciences (Geologische Rundschau)* 97, 785–797.

638 Hochuli, P.A., Menegatti, A.P., Weissert, H., Riva, A., Erba, E., Premoli Silva I., 1999.
639 Episodes of high productivity and cooling in the early Aptian Alpine Tethys. *Geology*
640 27/7, 657–660.

641 Hueter, A., Huck, S., Bodin, S., Heimhofer, U., Weyer, S., Jochum, K. P., Immenhauser, A.,
642 2019. Central Tethyan platform-top hypoxia during Oceanic Anoxic Event 1a. *Climate*
643 *of the Past* 15, 1327–1344.

644 Jacquin, T., Rusciadelli, G., Amédro, F., Graciansky, P.-C. de, Magniez-Jannin, F., 1998. The
645 north-Atlantic cycle: an overview of second order transgressive-regressive facies
646 cycles in Western Europe. *In* P.-C. de Graciansky, J. Hardenbol, T. Jacquin and P.R.
647 Vail (Eds), *Cenozoic and Mesozoic Sequence Stratigraphy of European Basins*.
648 *S.E.P.M., Special Publication*, 60, 397-409.

649 Jenkyns, H.C., 2010. Geochemistry of oceanic anoxic events. *Geochemistry, Geophysics,*
650 *Geosystems*, 11, 3.

651 Keller, C.E., Hochuli, P.A., Weissert, H, Bernasconi, S.M., Giorgioni, M., Garcia, T.I., 2011.
652 A volcanically induced climate warming and floral change preceded the onset of
653 OAE1a (Early Cretaceous). *Palaeogeography, Palaeoclimatology, Palaeoecology* 305,
654 43–49.

655 Kuhnt, W., Holbourn, A., Moullade, M., 2011. Transient global cooling at the onset of early
656 Aptian oceanic anoxic event (OAE) 1a. *Geology* 39, 4, 323–326.

657 Kuhnt, W., Moullade, M., Masse, J.P., Erlenkeuser, H., 1998. Carbon isotope stratigraphy of
658 the lower Aptian historical stratotype at Cassis– La Bédoule (SE France): *Géologie*
659 *Méditerranéenne*, 25, 63–79.

660 Lafargue, E., Marquis, F., Pillot, D., 1998. Les applications de Rock-Eval 6 dans l’exploration
661 et la production des hydrocarbures, et dans les études de contamination des sols. *Oil*
662 *and Gas Science and Technology, Revue de l’Institut Français du Pétrole* 53, 421–
663 437.

664 Larson, R.L., Erba, E., 1999. Onset of the mid-Cretaceous greenhouse in the Barremian-
665 Aptian: igneous events and the biological, sedimentary and geochemical responses.
666 *Paleoceanography* 14, 663–678.

667 Leckie, R. M., Bralower, T. J., Cashman, R., 2002. Oceanic anoxic events and plankton
668 evolution: Biotic response to tectonic forcing during the mid-Cretaceous:
669 *Paleoceanography*, 17, 13-1-13–29.

670 Li, Y.X., Bralower, T.J., Montañez, I.P., Osleger, D.A., Arthur, M.A., Bice, D.M., Herbert,
671 T.D., Erba, E., Premoli Silva, I., 2008. Toward an orbital chronology for the early
672 Aptian Oceanic Anoxic Event (OAE1a, ~120 Ma). *Earth and Planetary Science Letters*
673 271, 88–100.

674 Lorenzen, J., Kuhnt, W., Holbourn, A., Flögel, S., Moullade, M., Tronchetti, G., 2013. A new
675 sediment core from the Bedoulian (Lower Aptian) stratotype at Roquefort-La Bédoule,
676 SE France. *Cretaceous Research* 39, 6–16.

677 Luciani, V., Cobianchi, M., Lupi, C., 2006. Regional record of a global oceanic anoxic event:
678 OAE1a on the Apulia Platform margin, Gargano Promontory, southern Italy.
679 *Cretaceous Research* 27, 754-772.

680 Mangenot, X., Gasparrini, M., Gerdes, A., Bonifacie, M., Rouchon, V., 2018. An emerging
681 thermochronometer for carbonate-bearing rocks: $\Delta 47$ / (U-Pb). *Geology* 46, 1067–
682 1070.

683 Masse, J. P., Bouaziz, S., Amon, E. O., Baraboshkin, E., Tarkowski, R., Bergerat, F.,
684 Sandulescu, M., Platel, J.P., Canérot, J., Guiraud, R., Poisson, A., Ziegler, M.,
685 Rimmele, G., Map 13. Early Aptian. (112-114 Ma) *Peri-Tethys programme,*
686 *paleogeographical atlas. Commission de la Carte Géologique du Monde/Commission*
687 *for the Geologic Map of the World, Paris, 2000.*

688 Maurer, F., van Buchem, F.S.P., Eberli, G.P., Pierson, B.J., Raven, M.J., Larsen, P.H., Al-
689 Hussein, M. I., Vincent, B., 2012. Late Aptian long-lived glacio-eustatic lowstand
690 recorded on the Arabian Plate. *Terra Nova* 25, 87-94.

691 Méhay, S., Keller, C. E., Bernasconi, S. M., Weissert, H., Erba, E., Bottini, C., Hochuli, P. A.,

692 2009. A volcanic CO₂ pulse triggered the Cretaceous Oceanic Anoxic Event 1a and a
693 biocalcification crisis. *Geology* 37, 819–822.

694 Menegatti, A.P., Weissert, H., Brown, R.S., Tyson, R.V., Farrimond, P., Strasser, A., Caron,
695 M., 1998. High-resolution $\delta^{13}\text{C}$ stratigraphy through the early Aptian “Livello Selli” in
696 the Alpine Tethys. *Paleoceanography* 13, (5), 530-545.

697 Meyer, R., 1976. Continental sedimentation, soil genesis and marine transgression in the basal
698 beds of the Cretaceous in the east of the Paris Basin. *Sedimentology* 23, 235-253.

699 Millán, M.I., Weissert, H.J., López-Horgue, M.A., 2014. Expression of the late Aptian cold
700 snaps and the OAE1b in a highly subsiding carbonate platform (Aralar, northern
701 Spain). *Palaeogeography, Palaeoclimatology, Palaeoecology* 411, 167–179

702 Moore, D.M., Reynolds, R.C., 1997. X-Ray Diffraction and the Identification and Analysis of
703 Clay Minerals. Oxford University Press, New York, 378 p.

704 Mutterlose, J., Bornemann, A., Herrle, J.O., 2009. The Aptian – Albian cold snap: Evidence
705 for "mid" Cretaceous icehouse interludes *Neues Jahrbuch für Geologie und*
706 *Paläontologie - Abhandlungen*, 252, 217-225.

707 Mutterlose, J., Bottini, C., Schouten, S., Sinninghe Damsté, J. S., 2014. High sea-surface
708 temperatures during the early Aptian Oceanic Anoxic Event 1a in the boreal realm.
709 *Geology* 42, 439-442.

710 Mutterlose, J., Malkoc, M., Schouten, S., Sinninghe Damsté, J. S., Forster, A., 2010. TEX86
711 and stable $\delta^{18}\text{O}$ paleothermometry of Early Cretaceous sediments: implications for
712 belemnite ecology and paleotemperature proxy application. *Earth and Planetary*
713 *Science Letters* 298, 286–298.

714 Naafs, B. D. A., Castro, J. M., De Gea, G. A., Quijano, M. L., Schmidt, D. N., Pancost, R. D.,
715 2016. Gradual and sustained carbon dioxide release during Aptian Oceanic Anoxic
716 Event 1a. *Nature Geoscience* 9, 135–139.

717 Naafs, B.D.A., Pancost, R.D., 2016. Sea-surface temperature evolution across Aptian Oceanic
718 Anoxic Event 1a. *Geology* 44, 959–962.

719 Najarro, M., Rosales, I., Martín-Chivelet, J., 2011. Major palaeoenvironmental perturbation in
720 an Early Aptian carbonate platform: Prelude of the Oceanic Anoxic Event 1a?
721 *Sedimentary Geology* 235 50–71

722 O'Brien, C.L., Robinson, S.A., Pancost, R.D et al., 2017. Cretaceous sea-surface temperature
723 evolution: Constraints from TEX86 and planktonic foraminiferal oxygen isotopes.
724 *Earth-Science Reviews* 172, 224-247.

725 Pellenard, P., Deconinck, J.F., Marchand, D., Thierry, J., Fortwengler, D., Vigneron, G.,
726 1999. Contrôle géodynamique de la sédimentation argileuse du Callovien-Oxfordien
727 moyen dans l'Est du Bassin de Paris : influence eustatique et volcanique *Comptes*
728 *Rendus de l'Académie des Sciences, Paris* 328, 807-813

729 Pellenard, P., Deconinck, J.F., 2006. Mineralogical variability of Callovo-Oxfordian clays
730 from the Paris Basin and the Subalpine Basin. *Compte Rendus Geoscience* 338, 854-
731 866.

732 Pictet, A., Delanoy, G., Adatte, T., Spangenberg, J.E., Baudouin, C., Boselli, P., Boselli,
733 Kindler, P., Föllmi, K.G., 2015. Three successive phases of platform demise during
734 the early Aptian and their association with the oceanic anoxic Selli episode (Ardèche,
735 France). *Palaeogeography, Palaeoclimatology, Palaeoecology* 418, 101-125.

736 Quesnel, F., 2003. Paleoweathering and paleosurfaces from northern and eastern France to
737 Belgium and Luxembourg: geometry, dating and geodynamic implications. *Géologie*
738 *de la France* 1, 95-104.

739 Radley, J.D., Allen, P., 2012. The Wealden (non-marine Lower Cretaceous) of the Weald
740 Sub-basin, southern England. *Proceedings of the Geologists' Association* 123, 245-
741 318.

742 Reboulet, S. compiler 2018. Report on the 6th International Meeting of the IUGS Lower
743 Cretaceous Ammonite Working Group, the « Kilian Group » (Vienna, Austria, 20 th
744 August 2017). *Cretaceous Research* 91, 100-110.

745 Robaszynski, F., Pomerol, B., Masure, E., Bellier, J.P., Deconinck, J.F., 2005. Stratigraphy
746 and stage boundaries in a type-section of the Late Cretaceous chalk from the East Paris
747 basin: The “Craie 700 boreholes”. *Cretaceous Research* 26, 2, 157-169.

748 Ruffell, A., McKinley, J.M., Worden, R.H., 2002. Comparison of clay mineral stratigraphy to
749 other proxy palaeoclimate indicators in the Mesozoic of NW Europe. *Philosophical
750 Transactions of the Royal Society London A* 360, 675-693.

751 Sanchez-Hernandez, Y., Maurasse, F.J.-M.R., 2016. The influence of regional factors in the
752 expression of oceanic anoxic event 1a (OAE1a) in the semi-restricted Organyà Basin,
753 south-central Pyrenees, Spain. *Palaeogeography, Palaeoclimatology, Palaeoecology*
754 441, 582–598.

755 Schlanger, S.O., Jenkyns, H.C., 1976. Cretaceous oceanic anoxic events: causes and
756 consequences. *Geologie en Mijnbouw* 55, (3-4), 179-184.

757 Schouten, S., Hopmans, E.C., Forster, A., van Breugel, Y., Kuypers, M.M.M., Sinninghe
758 Damsté J.S., 2003. Extremely high sea-surface temperatures at low latitudes during the
759 middle Cretaceous as revealed by archaeal membrane lipids. *Geology* 31, 12, 1069–
760 1072.

761 Socorro, J., Maurasse, F.J.-M.R., 2019. Continuous accumulation of organic matter-rich
762 sediments associated with Oceanic Anoxic Event 1a in the El Pujal section, Organyà
763 Basin, Catalunya Spain and its relation to episodic dysoxia. *Cretaceous Research* 95,
764 225-251.

765 Socorro, J., Maurasse, F.J.-M.R., 2020. Regional palaeoenvironmental influence on organic
766 matter sequestration and characteristics of carbon isotope segment C5 in a hemipelagic

767 sequence, Organyà Basin, northeast Spain. Depositional record, DOI:
768 10.1002/dep2.111.

769 Squires, R.L., Saul, L.R., 1997. Review of the bivalve genus *Plicatula* from Cretaceous and
770 lower Cenozoic strata of California and Baja California. *Journal of Paleontology* 71,
771 (2), 287-298.

772 Stein, M., Föllmi, K. B., Westermann, S., Godet, A., Adatte, T., Matera, V., Berner, Z., 2011.
773 Progressive palaeoenvironmental change during the Late Barremian–Early Aptian as
774 prelude to Oceanic Anoxic Event 1a: evidence from the Gorgo a Cerbara section
775 (Umbria-Marche basin, central Italy). *Palaeogeography, Palaeoclimatology,*
776 *Palaeoecology* 302, 396–406.

777 Tarduno, J.A., Sliter, W. V., Kroenke, L., Leckie, M., Mayer, H., Mahoney, J. J., Musgrave,
778 R., Storey, M., Winterer, E. L., 1991. Rapid Formation of Ontong Java Plateau by
779 Aptian Mantle Plume Volcanism. *Science* 254, 399-403.

780 Tejada, M. L. G., Suzuki, K., Kuroda, J., Coccioni, R., Mahoney, J. J., Ohkouchi, N.,
781 Sakamoto, T., Tatsumi, Y., 2009. Ontong Java Plateau eruption as a trigger for the
782 early Aptian oceanic anoxic event. *Geology* 37, 855–858.

783 Thiry, M., 2000. Palaeoclimatic interpretation of clay minerals in marine deposits: an outlook
784 from the continental origin. *Earth-Science Reviews* 49, (1-4), 201-221.

785 Thiry, M., Quesnel, F., Yans, J., Wyns, R., Vergari, A., Théveniaut, H., Simon-Coinçon, R.,
786 Ricordel, C., Moreau, M.G., Giot, D., Dupuis, C., Bruxelles, L., Barbarand, J., Baele,
787 J.M., 2006. Continental France and Belgium during the early Cretaceous:
788 paleoweatherings and paleolandforms. *Bulletin de la Société Géologique de France*
789 177, (3), 155-175.

790 Thiry, M., Simon-Coinçon, R., Quesnel, F. Wyns, R., 2005. Altération bauxitique associée
791 aux argiles à chailles sur la bordure sud-est du bassin de Paris. Bulletin de la Société
792 Géologique de France 176, (2), 199-214.

793 Torelli, M., Traby, R., Teles, V., Ducros, M., 2020. Thermal evolution of the intracratonic
794 Paris Basin: Insights from 3D basin modelling. Marine and Petroleum Geology 119,
795 104487.

796 Van Helmond, N.A.G.M., Sluijs, A., Sinninghe Damsté, J.S., Reichert, G.J., Voigt, S.,
797 Erbacher, J., Pross, J., Brinkhuis, H. 2015. Freshwater discharge controlled deposition
798 of Cenomanian–Turonian black shales on the NW European epicontinental shelf
799 (Wunstorf, northern Germany). Climate of the Past 11, 495–508.

800 Velde, B. 1989. Phyllosilicate formation in berthierine peloids and iron oolites. Geological
801 Society, London, Special Publications, 46, 3-8.

802 Vincent, B., van Buchem, F.S.P., Bulot, L.G., Immenhauser, A., Caron, M., Baghbani, D.,
803 Huc, A.Y., 2010. Carbon-isotope stratigraphy, biostratigraphy and organic matter
804 distribution in the Aptian – Lower Albian successions of southwest Iran (Dariyan and
805 Kazhdumi formations) GeoArabia Special Publication 4, 1, 139-197.

806 Westermann, S., Stein, M., Matera, V., Fiet, N., Fleitmann, D., Adatte, T., Föllmi, K.B., 2013.
807 Rapid changes in the redox conditions of the western Tethys Ocean during the early
808 Aptian oceanic anoxic event. Geochimica et Cosmochimica Acta 121, 467–486.

809 Wissler, L., Funk, H., Weissert, H., 2003. Response of Early Cretaceous carbonate platforms
810 to changes in atmospheric carbon dioxide levels. Palaeogeography, Palaeoclimatology,
811 Palaeoecology 200, 187-205.

812 Wortmann, U.G., Herrle, J.O., Weissert, H. 2004. Altered carbon cycling and coupled
813 changes in Early Cretaceous weathering patterns: Evidence from integrated carbon

814 isotope and sandstone records of the western Tethys. Earth and Planetary Science
815 Letters 220, 69-82.

816 Yans, J. 2003. An overview of the saprolites of Belgium and their potential kaolinitic supplies
817 to Mesozoic and Cainozoic sediments. Géologie de la France 1, 33-37.

818 Zakharov, Y.D., Baraboshkin, E.Y., Weissert, H., Michailova, I. A., Smyshlyaeva, O.P.,
819 Safronova, P. P., 2013. Late Barremian-early Aptian climate of the northern middle
820 latitudes: Stable isotope evidence from bivalve and cephalopod molluscs of the
821 Russian Platform. Cretaceous Research 44, 183-201.

822

823 Figure captions

824

825 Fig. 1. Palaeogeographic map modified from R. Blakey: <https://www2.nau.edu/rcb7/>.

826 AM = Armorican Massif, MC = Massif Central, LBM = London Brabant Massif, RM =
827 Rhenish Massif, BM = Bohemian Massif, CSM = Corso-Sardinia Massif, AB =
828 Algarve Basin, PB = Paris Basin, LSB = Lower Saxony Basin.

829

830 Fig. 2. Simplified geological map of the area to the east of the Paris Basin and location of the
831 AUB 121 borehole near Juzanvigny.

832

833 Fig. 3. Lithology of the AUB 121 borehole from the lower Barremian “Argiles ostréennes”
834 Formation to the lowermost part of the “Argiles tégulines de Courcelles” Formation
835 (lower Albian) (modified after Amédéo et al., 2017). The lower Aptian Argiles à
836 Plicatules Formation comprises three distinct lithological units and are dated by
837 ammonites. The *deshayesi* and *furcata* ammonite Zones are clearly identified while the

838 lowermost part of the formation may belong to the *forbesi* Zone (see text). (A.P. =
839 Argiles à Plicatules).

840

841 Fig. 4. Base of the “Argiles à Plicatules” Formation. A. Thin section showing an iron oolite in
842 a clayey matrix with quartz grains (Q) (sample AUB 121 116.70 m). B. sample AUB
843 121, at an altitude of 116.60 m, shows abundant plant debris and notably *Weichselia*
844 *reticulata*. C. Picture of the core showing the top of Unit 1 (grey clays) with the
845 prominent shelly beds, and the base of Unit 2 (grey-brown clays).

846

847 Fig. 5. CaCO₃ content, %C_{org} and δ¹³C_{org} stratigraphic trends along the “Argiles à Plicatules”
848 Formation. The prominent δ¹³C_{org} negative excursion occurring prior to the OAE1a is
849 compared with the δ¹³C_{org} of the Roter Sattel reference section. Most of the segments
850 (C2 to C7) defined by Menegatti et al. (1998) are recognised in the Argiles à Plicatules
851 Formation.

852 W.F. = Wealden facies, *D. forb* = *Deshayesites forbesi*, Barr. = Barremian, Alb. = Albian.

853 MFS = Maximum Flooding Surface, TST = Transgressive System tract, HST = Highstand
854 system tract.

855

856 Fig. 6. Clay mineralogy of the Argiles à Plicatules Formation (the proportions of chlorite,
857 approximately 5% throughout the formation, are not plotted). *D. forb* = *Deshayesites*
858 *forbesi*, W.F. = Wealden facies.

859 MFS = Maximum Flooding Surface, TST = Transgressive System tract, HST = Highstand
860 system tract.

861

862 Fig. 7. Early Aptian climate trends deduced from $\delta^{13}\text{C}_{\text{org}}$ and kaolinite content through the
863 Argiles à Plicatules Formation.

864 MFS = Maximum Flooding Surface, TST = Transgressive System tract, HST = Highstand
865 system tract.

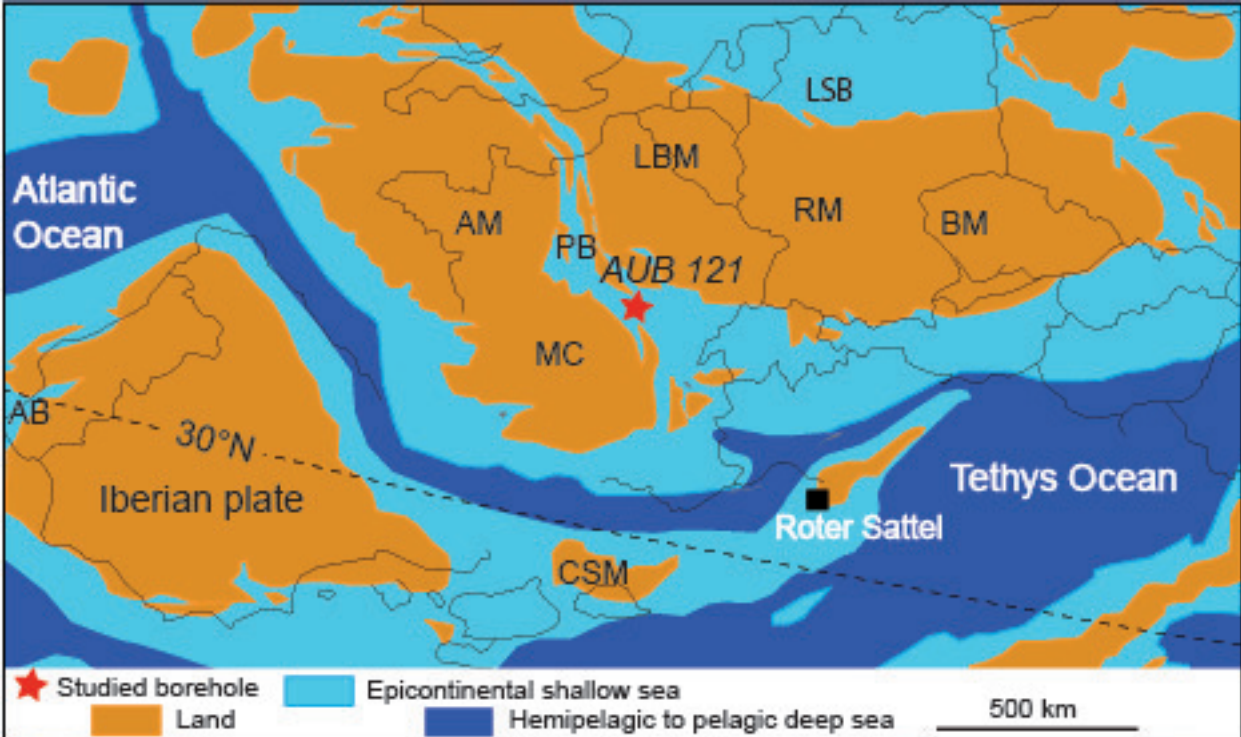
866

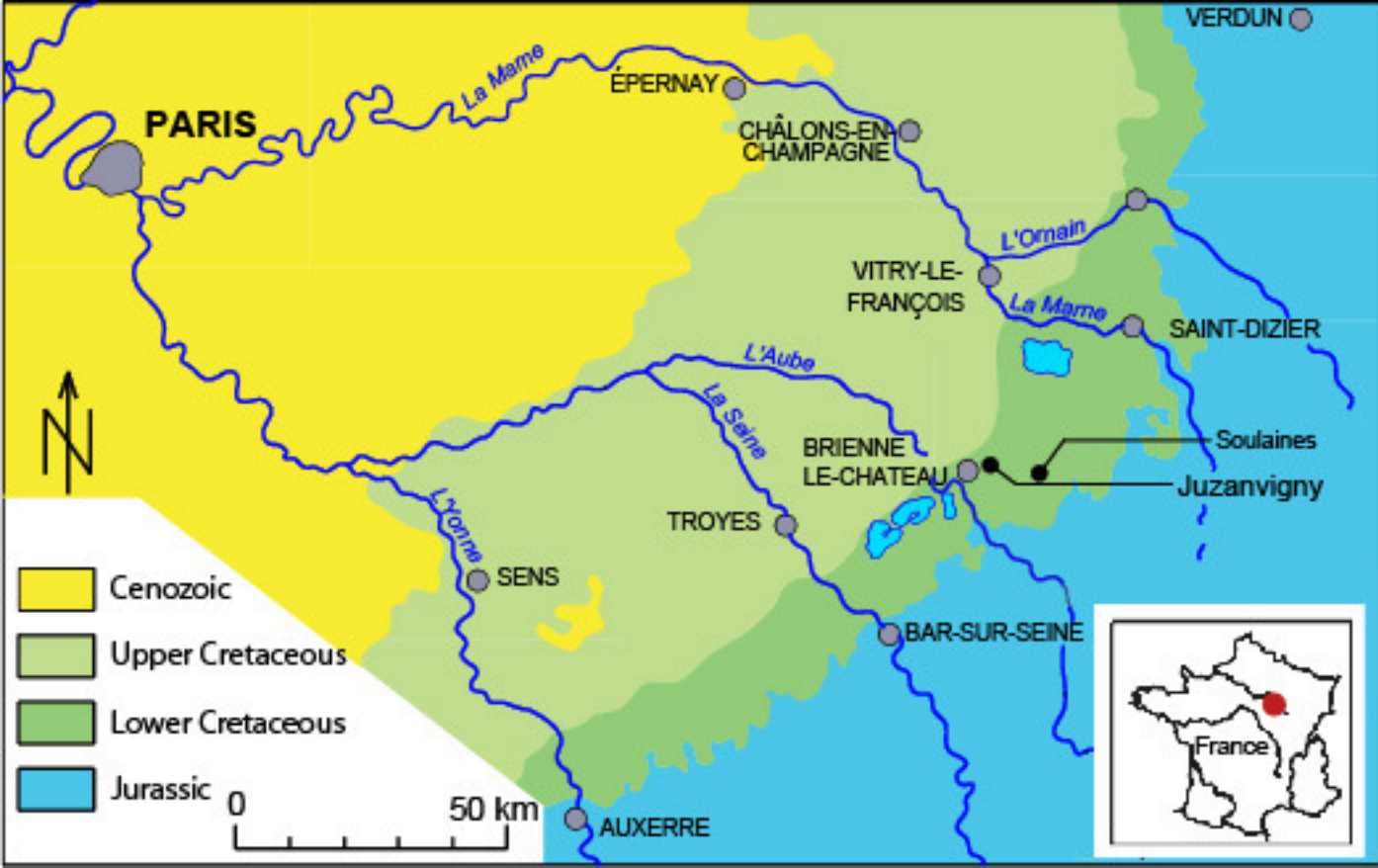
867

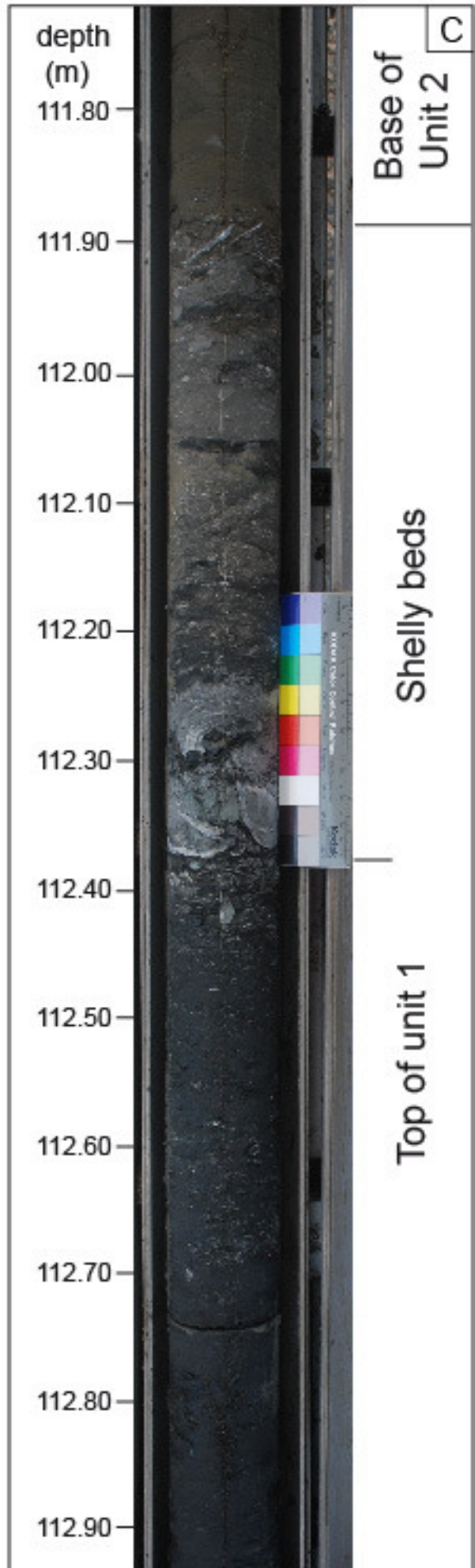
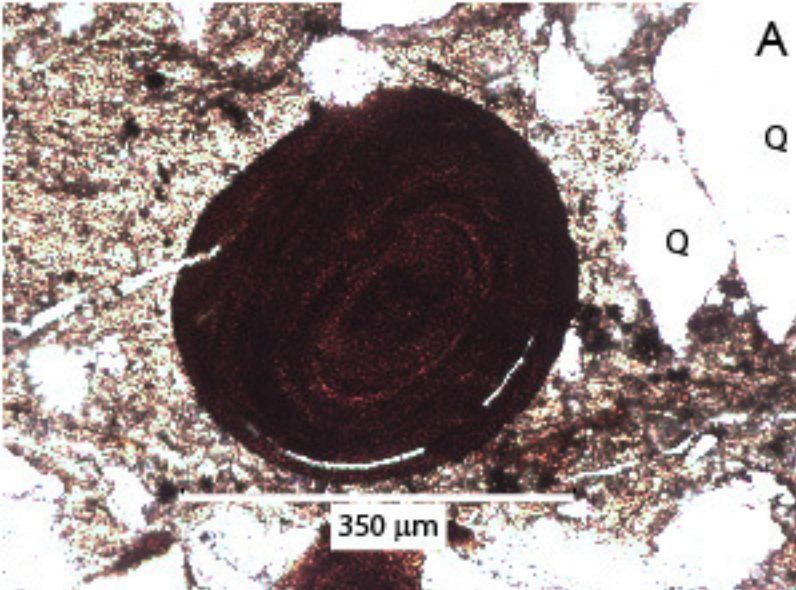
868 Table 1. Rock-Eval data of the studied samples (TOC = Total Organic Carbon, OI = Oxygen
869 index, HI, Hydrogen index).

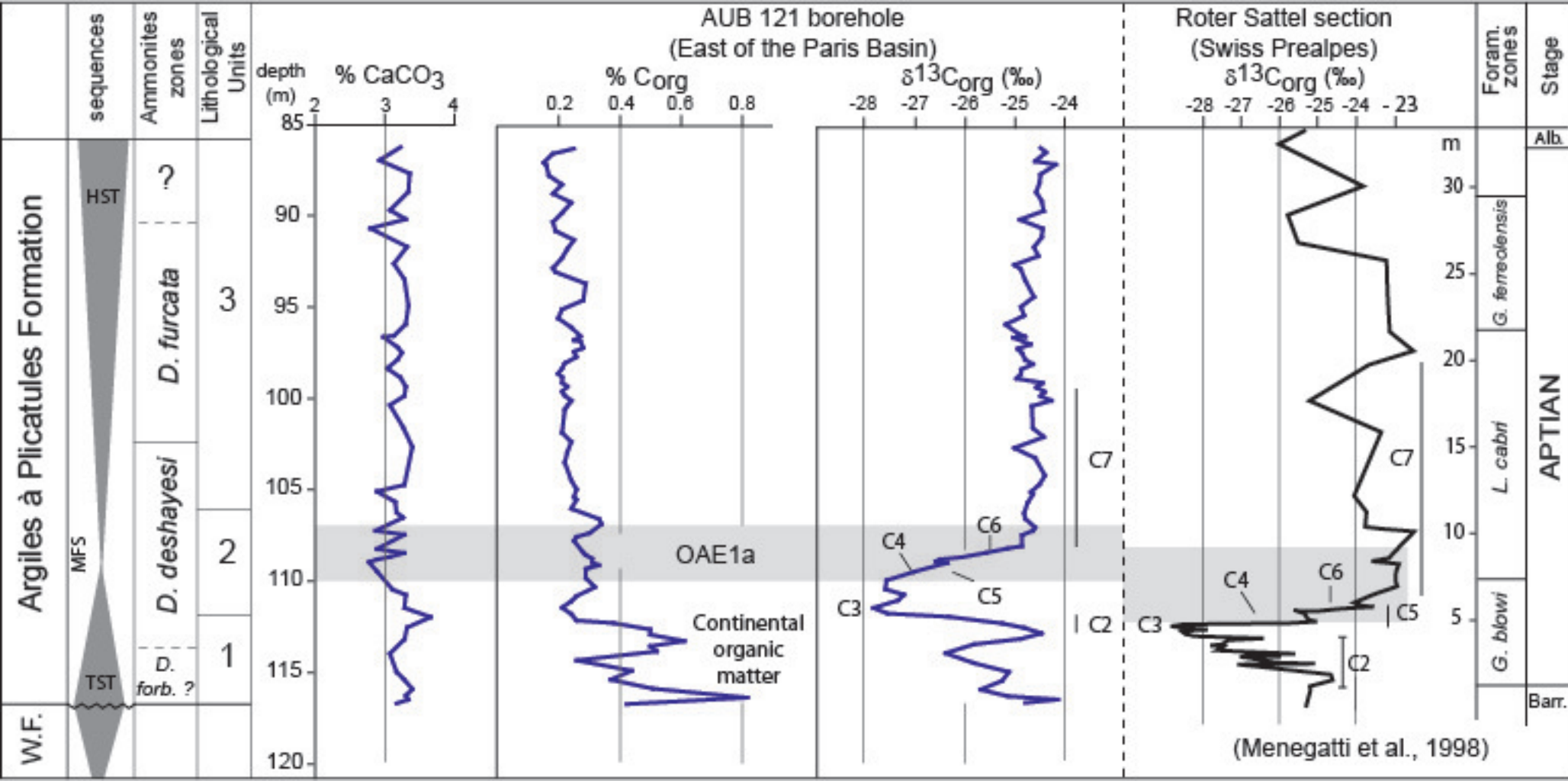
870

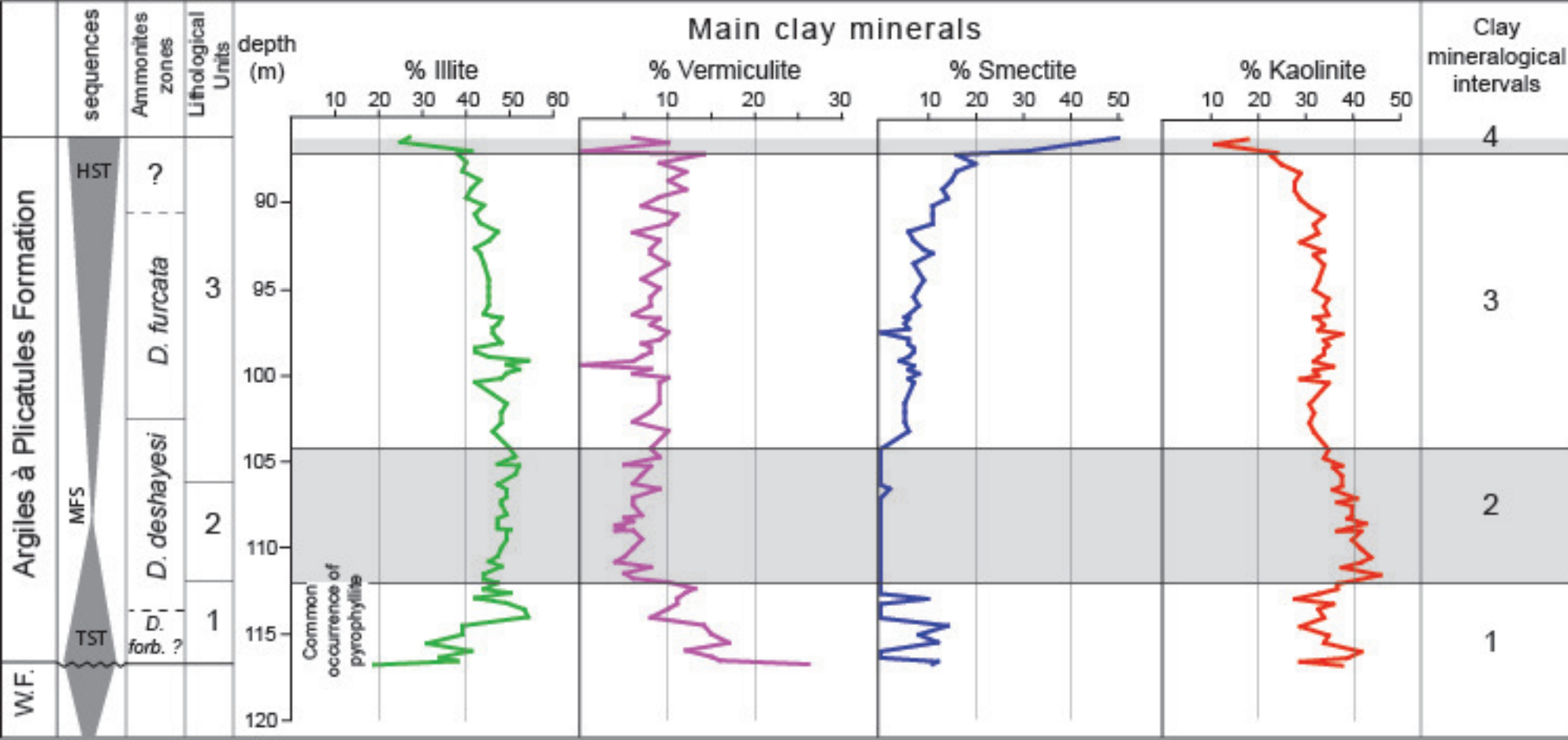
871

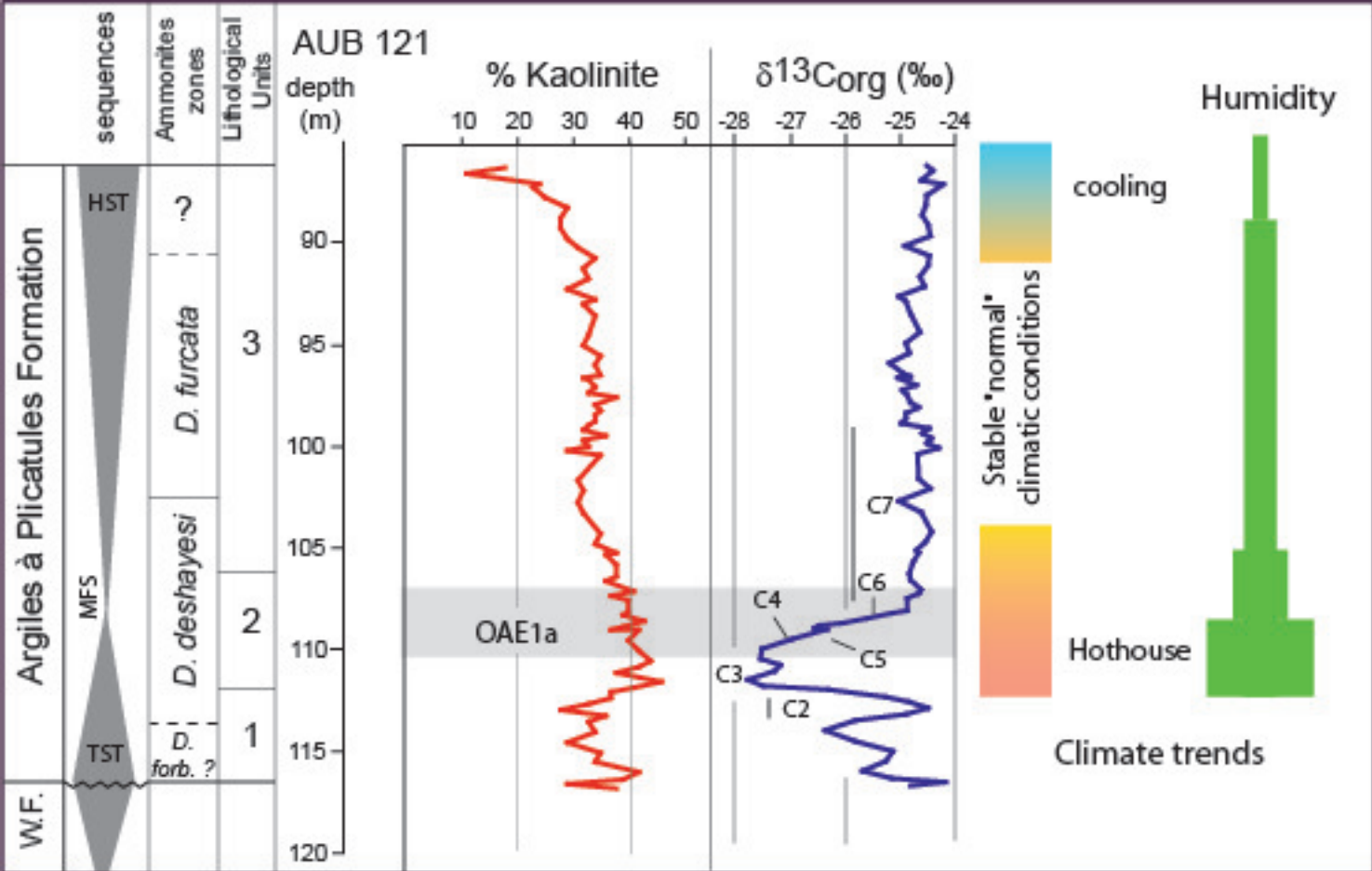












Sample (depth m)	reliable Tmax (°C)	TOC(%)	HI (mgHC/g TOC)	OI (mgCO2/gTOC)
86.45		0.13	54	208
87.12		0.1	70	250
88.15		0.18	67	233
89.15		0.18	33	139
90.15		0.13	54	269
91.15		0.18	39	144
92.15		0.15	33	233
92.90		0.12	52	300
94.42		0.23	43	135
96.42		0.22	45	132
97.00		0.22	45	132
97.50		0.21	33	133
98.13		0.17	53	194
98.63		0.17	53	218
99.13		0.18	44	172
99.63		0.18	36	180
100.13		0.18	44	128
101.10		0.17	41	135
102.10	398	0.21	100	152
103.23		0.17	47	141
104.23		0.2	50	150
105.23		0.19	63	221
107.07		0.21	48	190
108.00		0.16	59	256
110.00	418	0.23	83	148
111.00		0.17	53	229
111.80		0.13	77	277
112.35		0.26	38	92
112.92	384	0.52	56	92
113.52	419	0.44	34	139
114.52b	365	0.38	53	216
114.52a	394	0.4	55	258
115.50		0.42	26	129